

Catalytic partial oxidation of methane to synthesis gas over Ni–CeO₂

Tianli Zhu, Maria Flytzani-Stephanopoulos*

Department of Chemical Engineering, Tufts University, Medford, MA 02155, USA

Received 3 February 2000; received in revised form 14 July 2000; accepted 16 July 2000

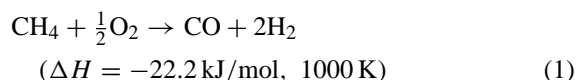
Abstract

The partial oxidation of methane to syngas was studied in this work over Ni-containing ceria catalysts with nickel content of 5, 10 and 20 at.% at atmospheric pressure. All catalysts, in the as prepared state, showed similar activity and CO selectivity at $T \geq 550^\circ\text{C}$. Catalyst pre-reduction was not required. Reaction mixtures were dilute, containing 3 mol% CH₄ and 1.5 mol% O₂. Methane conversion and CO selectivity approached their respective thermodynamic equilibrium values above 550°C. The H₂/CO ratio was equal to 2 at $T > 600^\circ\text{C}$. In the range 0.54–0.04 g s/cm³ (STP), contact time effects were absent in partial oxidation of methane over the 5 at.% Ni–Ce(La)O_x catalyst. The phase composition, nickel dispersion and carbon deposition on the catalysts were investigated by various characterization techniques, including XRD, STEM/EDS, XPS and TPO analyses. The 5 at.% Ni–Ce(La)O_x catalyst, comprising highly dispersed nickel oxide in ceria, showed excellent resistance to carbon deposition and stable performance during 100 h-on-stream at 650°C. On the other hand, high-content (>10 at.%) nickel in ceria, comprising both dispersed nickel and bulk nickel oxide particles, was unstable even after a much shorter time-on-stream; carbon deposition was clearly the cause of this performance instability. © 2001 Elsevier Science B.V. All rights reserved.

Keywords: Partial oxidation of methane; Synthesis gas; Nickel catalysts; Ceria; Carbon deposition

1. Introduction

Natural gas is the cleanest fossil fuel and the most desirable feedstock for chemicals production. Steam reforming of natural gas is widely used to produce synthesis gas for various chemicals. The catalytic partial oxidation of methane (POM) to synthesis gas:



has been under intense study [1–9] as a potential alternative to the highly endothermic steam reforming process. Adoption of POM would result in energy savings. The stoichiometry of reaction (1) with a product molar ratio H₂/CO = 2, is suitable for Fisher–Tropsch and methanol synthesis. Of course, in conjunction with the water–gas–shift reaction, POM may be used to produce H₂ for fuel cell applications.

The first-row transition metals (Ni, Co and Fe) [2–5] and the noble metals (Ru, Rh, Pd, Pt, Ir) [1,6–9] have been reported as active catalysts for the partial oxidation of methane. Several problems, including the pyrophoric nature and deactivation of these catalysts remain to be solved. The Ni-based catalyst is the most studied one for POM due to its low cost. However, a rapid deactivation due to carbon deposition

* Corresponding author.

E-mail address: mstephanopoulos@infonet.tufts.edu (M. Flytzani-Stephanopoulos).

or metal loss at high temperature has been reported for nickel catalysts. Carbon deposition mainly comes from methane decomposition: $\text{CH}_4 \rightarrow \text{C}_s + 2\text{H}_2$; and CO disproportionation: $2\text{CO} \rightarrow \text{C}_s + \text{CO}_2$, where C_s refers to surface carbon. The former dominates at high temperature, while the latter is a low-temperature pathway to carbon. Claridge et al. [10] showed that methane decomposition is the principal route for carbon formation over a supported nickel catalyst at the typical methane partial oxidation temperature of 1050 K. Both ‘whisker’ and ‘encapsulated’ forms of carbon were present on a catalyst with a high Ni loading. Recent studies have focused on developing a highly active and stable catalyst for partial oxidation. Different additives were studied for the Ni–Al₂O₃ system [11–14]. Mixed metal oxides, NiO–MgO solid solutions [15–17], Ni–BaTiO₃ [18], Ni–Mg–Cr–La–O [19] and Ca_{0.8}Sr_{0.2}Ti_{1.0}Ni_{0.2} [20] mixed oxides, were reported to be highly active and selective catalysts at high space velocity (10⁵–10⁶ ml/g h) and high temperature (>700°C) with improved carbon resistance.

Ceria, a stable fluorite-type oxide, has been studied for various reactions utilizing its redox properties, which can be further enhanced in the presence of a metal or metal oxide [21–27]. Ceria-based materials, such as CuO–CeO₂, have been mostly examined as active catalysts for total oxidation, such as CO oxidation [25,28–31] and CH₄ combustion [24,29,30,32]. Recently, Otsuka et al. [33–35] showed that ceria is able to directly convert methane to syngas with H₂/CO = 2 at temperatures higher than 600°C. Ceria has also been examined as a promoter of both the activity and selectivity of supported Ni or Pt catalysts for partial oxidation of methane [11–12] or CO₂ reforming of methane [36,37]. Ceria-supported Ni with high Ni-loading (13 wt.%) was reported by Tang et al. [17] to be an active catalyst for POM at $T = 750^\circ\text{C}$. However, this catalyst rapidly deactivates due to carbon deposition.

In this paper, we report on the activity/selectivity and stability of Ni-ceria catalysts, with Ni content ranging from 5 to 20 at.% (corresponding to 2.5–10 wt.%), for the partial oxidation of CH₄ to syngas in the medium-high temperature range 550–700°C at atmospheric pressure. Parametric studies included the effect of contact time and catalyst pre-reduction. Carbon deposition was checked by

temperature-programmed oxidation, on-line NDIR–CO₂ analysis, and post-reaction surface analysis of the catalysts. Selected samples were characterized by XRD, XPS and STEM/EDS.

2. Experimental

Bulk Ni–Ce(La)O_x catalysts were synthesized by the urea coprecipitation/gelation method using metal nitrates and urea [30,38]. This method provides well-dispersed and homogeneous mixed metal oxides. Supported Ni/Ce(La)O_x catalysts were prepared by impregnation of Ce(La)O_x, itself prepared by the urea coprecipitation/gelation method, with a solution of nickel nitrate of appropriate concentration, corresponding in volume to the total pore volume of the support (incipient wetness). For the materials reported in this work, the pore volume was about 0.10 cm³/g. All catalysts were calcined in air at 650°C for 3 h. The dopant level in all materials is expressed in atomic metal percent, e.g. for lanthanum, as $\text{La}/(\text{La} + \text{Ce}) \times 100\%$.

For bulk composition analysis, the catalyst powder was dissolved in a 70% HNO₃ acid solution (A.C.S. reagent) and diluted with deionized water. The resulting solution was analyzed by inductively coupled plasma (ICP) atomic emission spectrometry (Perkin Elmer Plasma 40). The BET surface area of the sample was measured by single-point N₂ adsorption/desorption on a Micromeritics Pulse ChemiSorb 2705 instrument. X-ray powder diffraction (XRD) analysis was performed on a Rigaku 300 instrument. Copper Kα1 radiation was used with a power setting of 60 kV and 300 mA. The surface composition of the catalysts was analyzed by X-ray photoelectron spectroscopy (XPS) on a Perkin Elmer 5100C system. All measurements were carried out at room temperature without any sample pre-treatment. Binding energies were adjusted relative to C1s at 284.6 eV. A magnesium X-ray source was primarily used in this work. The X-ray generator power was typically set at 15 kV and 20 mA. The catalyst microstructure was studied by a Vacuum Generators HB 603 scanning transmission electron microscope (STEM) equipped with a X-ray microprobe of 0.14 nm optimum resolution for energy dispersive X-ray spectroscopy (EDS). The catalyst powder was dispersed on a nickel or copper

grid coated with a carbon film and elemental maps were obtained on a 128×128 data matrix.

Reaction tests were conducted in a packed-bed quartz microreactor tube (I.D. = 1 cm) operated isothermally at atmospheric pressure. Typically, 300 mg of sample in fine powder form ($< 150 \mu\text{m}$) was loaded on the quartz frit in the center of the reactor. The reactor tube was heated inside a Lindberg electric furnace. The temperature was measured by a quartz tube-sheathed K-type thermocouple placed at the top of the packed bed, and was controlled by a Wizard temperature controller. Feed gases with $\text{CH}_4/\text{O}_2 = 2$ were mixed and diluted with He upstream of the reactor. Dilute gas mixtures were used (3% CH_4) at a typical flow rate of $100 \text{ cm}^3/\text{min}$ (STP). The reactor was operated isothermally. The reacting gases were all certified calibration gas mixtures with helium (99.999%, Middlesex), used without any further purification. The feed and product gas streams were analyzed by a HP 6890A gas chromatograph (GC) equipped with a TCD detector. A packed column, Carbosphere 80/100 (Alltech), was used to separate CH_4 , CO, CO_2 and O_2 . Occasionally, a molecular sieve 5A column (Alltech), which separates H_2 , O_2 , CH_4 and CO, was used to check the H_2/CO ratio. A cold trap at the outlet of the reactor was used to condense out any water from the product gas stream. Since very dilute gas mixtures were used, the CO yield, Y-CO, was calculated from the ratio of CO produced to methane inlet concentration without any volume correction. The selectivity to CO, S-CO, is defined as $\text{Y-CO}/\text{X-CH}_4$, where the latter term is the methane conversion.

Temperature-programmed reduction (TPR) of the as-prepared catalysts in a CH_4 -He gas mixture was carried out in a Cahn TG 121 thermogravimetric analyzer (TGA). Samples were preheated to 500°C in a 5% O_2 -He mixture ($200 \text{ cm}^3/\text{min}$) for 30 min. After cooling down to room temperature in the O_2 -He mixture followed by flushing in He for 15 min, TPR in a 5% CH_4 -He mixture began. A heating rate of $10^\circ\text{C}/\text{min}$ was used. The catalyst weight change in the TGA was continuously recorded up to 750°C . CH_4 -TPR was also conducted in the microreactor with on-line mass spectrometry (MS) using a residual gas analyzer (MKS-model RS-1). For this study, 150 mg of catalyst was loaded into the quartz tube reactor. The catalyst was pre-treated in 10% O_2 -He at 500°C for 30 min and then cooled down in the

same stream to room temperature. The catalyst was then flushed with He for 15 min and heated in a 2% CH_4 -He gas mixture at a heating rate of $5^\circ\text{C}/\text{min}$ to 750°C . The flow rate of the reducing gas was typically $50 \text{ cm}^3/\text{min}$ (STP). The effluent gas composition was followed by MS.

Temperature-programmed oxidation (TPO), carried out in the TGA, was used to check for carbon deposition on the used catalysts. About 10 mg sample was loaded in the quartz pan. The sample was pre-heated to 400°C for 30 min in He, then cooled down to room temperature. TPO began by heating up the sample in 5% O_2 -He ($200 \text{ cm}^3/\text{min}$) at a heating rate of $5^\circ\text{C}/\text{min}$. The weight change of the catalyst was recorded up to 800°C . TPO was also run in the microreactor (20% O_2 -He, $50 \text{ cm}^3/\text{min}$, heating rate $5^\circ\text{C}/\text{min}$) with the product gas monitored for CO_2 by an on-line non-dispersive infra-red (NDIR) analyzer (Beckman 864).

3. Results and discussion

3.1. Catalyst composition and activity

In this work, all catalysts were doped with ~ 4 at.% lanthanum. La dopant was used to achieve high surface area and nanocrystalline ceria [24], which is denoted as $\text{Ce}(\text{La})\text{O}_x$ throughout the paper. Table 1 lists the BET surface area of various catalyst compositions, and particle size determined by XRD. Also, Table 1 shows the effect of La addition on the lattice parameter of ceria. Oxide solid solution was formed in La-doped CeO_2 with a dopant level of 4–20 at.% [39]. For the 5 at.% Ni-Ce(La) O_x , only the fluorite oxide-type structure was identified on this sample, as shown in Fig. 1. No separate NiO phases were discernible by XRD. However, STEM/EDS elemental mapping of the as prepared 5 at.% Ni-Ce(La) O_x (Fig. 2) identified nickel clusters well dispersed within the CeO_2 matrix. Therefore, at low Ni content, nickel oxide was present in ceria, but, in nanoparticle form. At higher metal content (≥ 10 at.% Ni), bulk NiO particles ($\sim 20 \text{ nm}$) were also present, as identified by both XRD and STEM/EDS (Figs. 1 and 2). The ceria lattice parameters obtained from the XRD reflections of Ni-Ce(La) O_x catalysts are shown in Table 1. These values are close to the lattice parameter of $\text{Ce}(\text{La})\text{O}_x$, within experimental error. Furthermore,

Table 1
Physical properties of ceria-based catalysts^a

Sample	BET surface area (m ² /g)		Particle size (nm) ^d based on CeO ₂ (1 1 1)		CeO ₂ lattice parameter α (Å) ^f
	Fresh	Used ^e	Fresh	Used ^e	
CeO ₂ ^b	75		10.2	n.a.	5.411
Ce(4 at.% La)O _x ^b	90	24.9	8.8	n.a.	5.421
5 at.% Ni–Ce(La)O _x ^b	99	27.0 ^g	7.4	11.7 ^g	5.419
10 at.% Ni/Ce(La)O _x ^c	61	29.1	9.3	13.2	5.423
20 at.% Ni/Ce(La)O _x ^c	62	33.4	9.0	12.7	5.424

^a Calcined in air at 650°C for 3 h.

^b Prepared by the urea coprecipitation/gelation method.

^c Prepared by incipient wetness impregnation.

^d Determined from CeO₂ (1 1 1) reflection according to the Scherrer equation [56].

^e Unless otherwise specified, all samples were used up to 700°C for 16 h, CH₄/O₂ = 2, contact time = 0.18 g s/cm³.

^f Calculated from ceria (1 1 1) reflection from the equation $\alpha = \sqrt{h^2 + k^2 + l^2}(\lambda/2 \sin \theta)$ [56].

^g After 100 h-on-stream at 650°C, CH₄/O₂ = 2, contact time = 0.18 g s/cm³.

no obvious change in lattice parameter was detected in other Ni–CeO₂ samples, all prepared by the urea coprecipitation/gelation technique with various nickel loadings. Therefore, no oxide solid solution formation of Ni with CeO₂ is indicated by the XRD analysis.

Table 2 shows the surface composition of Ni-containing ceria materials based on the XPS findings. The surface content of Ni was found to be a little less than the bulk in samples containing both 5 and 10 at.% Ni. This is consistent with the XPS results of Lamonier et al. [27]. However, these researchers also reported that an oxide solid solution formed in Ni–CeO₂ with substitution of Ni²⁺ ions in the ceria lattice. However, the shift of 2θ in their XRD measurement was very small ($\Delta(2\theta) < 0.07$ for a material with 15 at.% Ni–CeO₂) and was not captured by

the XRD analysis carried out in this work (Table 1, Fig. 1). For the 10 at.% Ni/Ce(La)O_x prepared by impregnation, surface enrichment in Ni was observed (Table 2). About four times more nickel was on the surface than in the bulk, comparable to that reported by Tang et al. for their 13 wt.% Ni/CeO₂ sample [17]. Therefore, in the catalysts prepared by the urea coprecipitation/gelation, nickel may be more uniformly dispersed in ceria. Fig. 3 shows the Ni2p spectra of 10 at.% Ni/Ce(La)O_x and 5 at.% Ni–CeO₂, the latter after 10 h-long data acquisition in order to obtain a good signal-to-noise ratio since the nickel signal was very weak. The spectra show that nickel is in the divalent state in ceria.

The catalyst activity for partial oxidation of methane (POM) to syngas was tested in a dilute mixture (3% CH₄–1.5% O₂–He) in the temperature range of 500–700°C. A dilute reactant gas mixture was used to avoid hot-spots in the packed catalyst bed and for better temperature control. Ce(La)O_x with La dopant from 4 to 20 at.% is active for total oxidation of methane to CO₂ and H₂O over this temperature range [24]. Partial methane oxidation products, i.e. CO and H₂, were observed on Ce(La)O_x only at temperatures higher than 650°C with about 5% CO yield obtained at 750°C, as shown in Fig. 4.

On the other hand, addition of a small amount of Ni into Ce(4 at.% La)O_x caused a dramatic improvement in POM activity. Fig. 4 shows the CH₄ conversion and selectivity to CO plotted versus temperature for 5 at.% Ni–Ce(La)O_x at a contact time of 0.18 g s/cm³ ($\sim 40,000 \text{ h}^{-1}$ (STP)). The catalyst

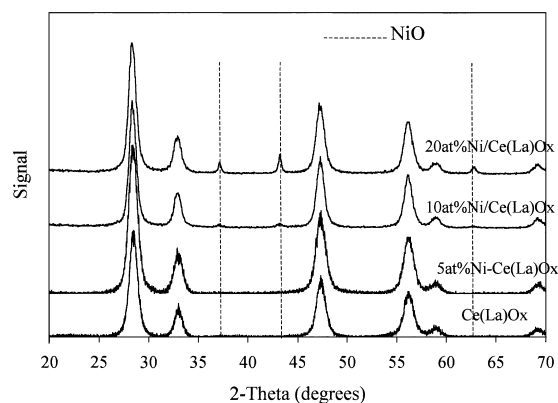


Fig. 1. XRD patterns of Ni modified Ce(La)O_x; peaks without lines are due to the reflections of ceria; as-prepared catalysts (Table 1).

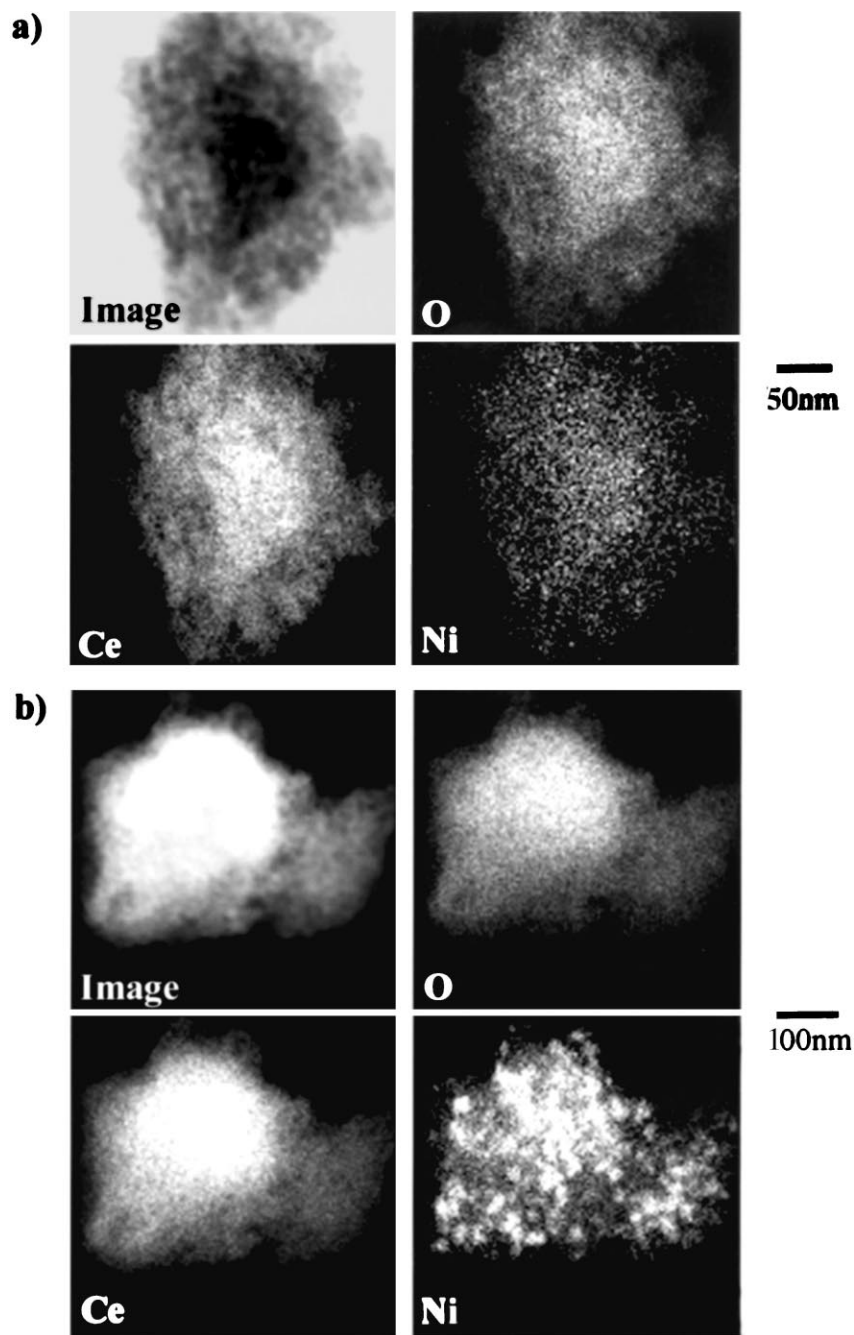


Fig. 2. STEM/EDS of Ni-modified Ce(La)O_x (a) 5 at.% Ni- Ce(La)O_x ; (b) 10 at.% Ni/ Ce(La)O_x ; as-prepared (Table 1).

Table 2
Bulk and surface composition of Ni–Ce(La)O_x

Sample	Surface composition ^c		Bulk composition ^d	
	Ni/Ce	La/Ce	Ni/Ce	La/Ce
5 at.% Ni–Ce(La)O _x ^a	0.042	0.023	0.052	0.040
10 at.% Ni–Ce(La)O _x ^a	0.061	0.091	0.111	0.068
10 at.% Ni/Ce(La)O _x ^b	0.403	0.024	0.116	0.052
20 at.% Ni/Ce(La)O _x ^b	n.a.	n.a.	0.262	0.060

^a Prepared by the urea coprecipitation/gelation method [30,38]; calcined at 650°C, 3 h.

^b Prepared by incipient wetness impregnation of Ce(La)O_x; calcined at 650°C, 3 h.

^c Determined by XPS of the 650°C-calcined samples.

^d Analyzed by ICP.

was not pre-reduced and the reactant gas mixture was directly introduced at 500°C. Oxygen was completely converted at all temperatures tested. The POM light-off temperature, where CO and H₂ start to be formed over 5 at.% Ni–Ce(La)O_x is ~550°C, while only complete oxidation products, CO₂ and H₂O, were formed at $T \leq 500^\circ\text{C}$. Methane conversion increased with temperature. At 650°C, ~94% methane conversion was achieved and the CO selectivity was ~86%, close to the equilibrium values calculated by the STANJAN program [40], as shown in Fig. 4. Complete oxidation products, i.e. CO₂ and H₂O, as well as syngas can be formed through various reactions [41] and were assumed to be present at equilibrium both in reference [41] and here using the STANJAN program. Equilibrium was attained at temperatures in

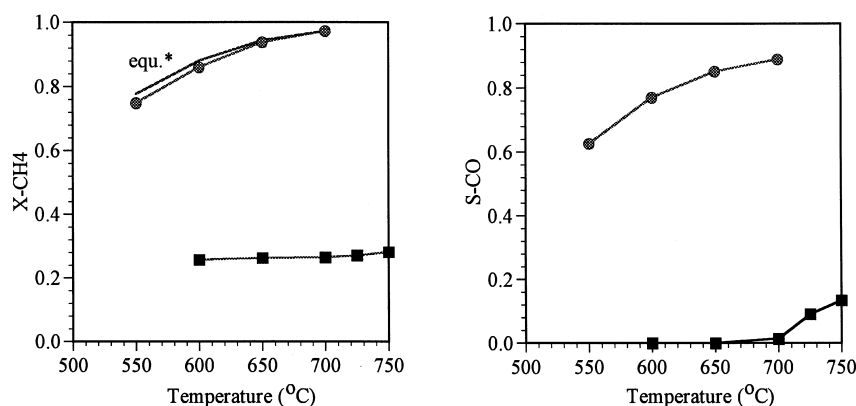


Fig. 4. CH₄ conversion and selectivity to CO in partial oxidation of methane over (■) Ce(La)O_x; (●) 5 at.% Ni–Ce(La)O_x catalysts (3% CH₄–1.5% O₂–He, 0.18 g s/cm³ (STP)); (*) equilibrium values calculated from the STANJAN program [40].

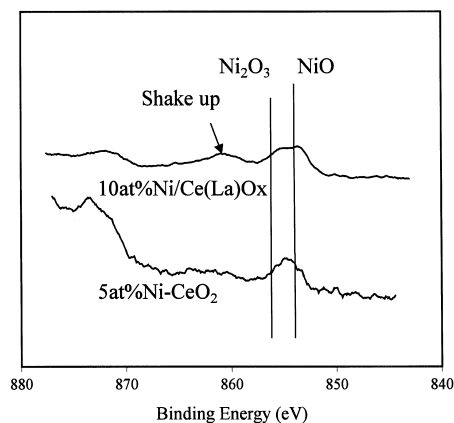


Fig. 3. Ni₂p XP spectra of (a) 5 at.% Ni–CeO₂; (b) 10 at.% Ni/Ce(La)O_x; as-prepared catalysts (Table 1).

the range 550–700°C. The carbon balance was better than 95%. The H₂/CO ratio was 2 ± 0.02 at high methane conversions.

Ni/Ce(La)O_x catalysts, prepared by impregnation with higher Ni loading, i.e. 10 and 20 at.% Ni/Ce(La)O_x, were also active for POM, as shown in Fig. 5. Without pre-reduction, the light-off temperature of 20 at.% Ni/Ce(La)O_x was ~650°C and hysteresis was observed in the fall-off mode. The light-off temperature of this material was lowered to ~550°C after the catalyst was pre-reduced in 10% H₂–He at 500°C for 1 h. The 20 at.% Ni/Ce(La)O_x material showed lower selectivity to CO than the 5 and 10 at.% Ni–Ce(La)O_x. The carbon balance with the former was about 88%,

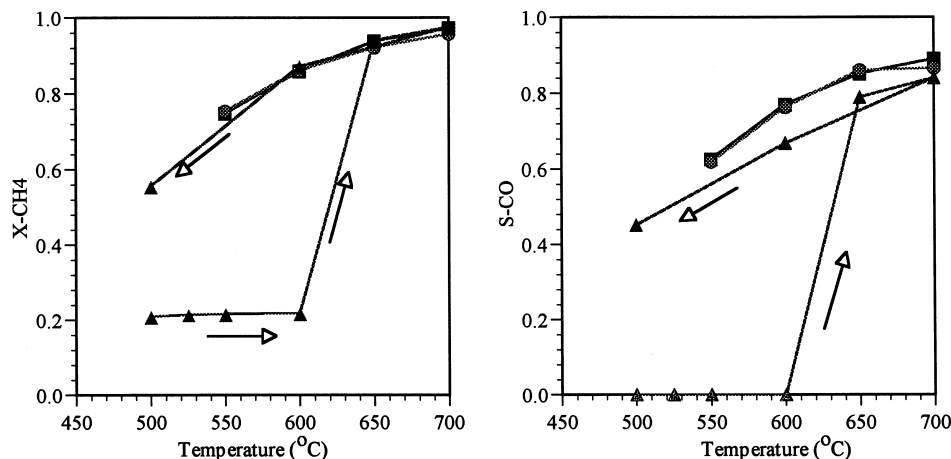


Fig. 5. CH₄ conversion and CO selectivity curves in partial oxidation of methane over (■) 5 at.% Ni-Ce(La)O_x; (●) 10 at.% Ni-Ce(La)O_x; (▲) 20 at.% Ni-Ce(La)O_x catalysts (3% CH₄-1.5% O₂-He, 0.18 g s/cm³ (STP)).

indicating that carbon deposition may have taken place on this material during reaction.

It is generally accepted that the active component in supported nickel catalysts for POM is metallic nickel [5]. Therefore, catalysts usually have to be pre-reduced. This is the case for the 20 at.% Ni/Ce(La)O_x catalyst, which had to be pre-reduced in order to be active for POM at low temperatures (550 and 600°C), Fig. 5. The unreduced catalyst showed POM activity only at $T \geq 650^\circ\text{C}$ in the light-off mode and then showed activity at low temperatures in the fall-off mode. On the other hand, as mentioned above, pre-reduction had no effect on the POM activity of 5 at.% Ni-Ce(La)O_x. Both the unreduced

and pre-reduced catalyst showed similar activity and selectivity for POM. However, even the 5 at.% Ni-Ce(La)O_x or the pre-reduced Ni-Ce(La)O_x catalysts showed activity at $T < 550^\circ\text{C}$ only after use in the reaction at $T \geq 550^\circ\text{C}$. Choudhary et al. [42] have observed similar behavior over their catalysts and suggested that the creation of active sites responsible for the low temperature activity/selectivity is due to further catalyst reduction and/or formation of surface carbon species. Adsorbed carbon has been suggested by some researchers to be the intermediate for the formation of CO [8,35].

Fig. 6 shows the effect of contact time on methane conversion and CO yield over 5 at.% Ni-Ce(La)O_x.

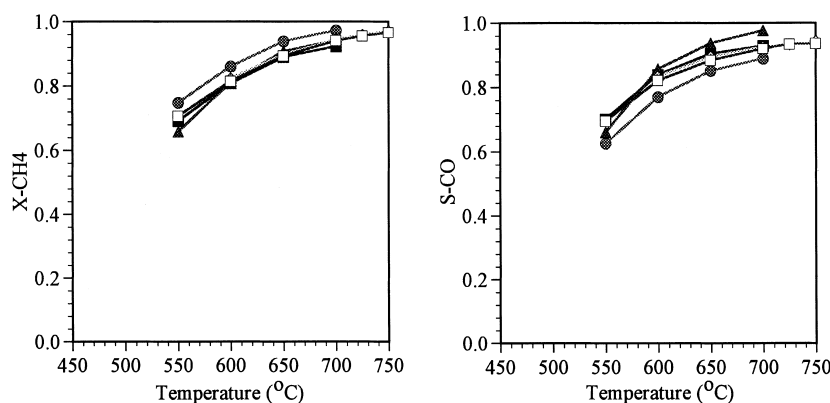


Fig. 6. Effect of contact time on CH₄ conversion and CO selectivity over 5 at.% Ni-Ce(La)O_x (■) 0.54 g s/cm³; (●) 0.18 g s/cm³; (▲) 0.12 g s/cm³; (◆) 0.06 g s/cm³; (□) 0.04 g s/cm³ (3% CH₄-1.5% O₂-He).

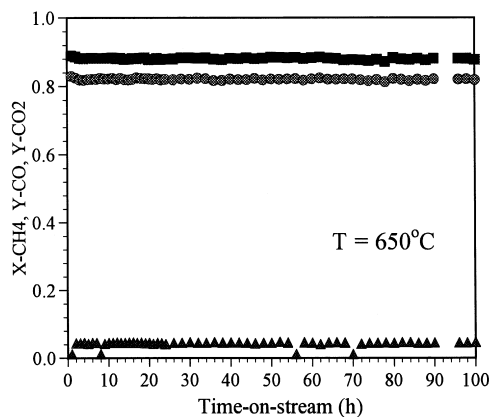


Fig. 7. Catalytic activity and stability of 5 at.% Ni-Ce(La) O_x at $T = 650^\circ\text{C}$ (■) X-CH $_4$; (●) Y-CO; (▲) Y-CO $_2$ (3% CH $_4$ -1.5% O $_2$ -He, 0.18 g s/cm 3 (STP)).

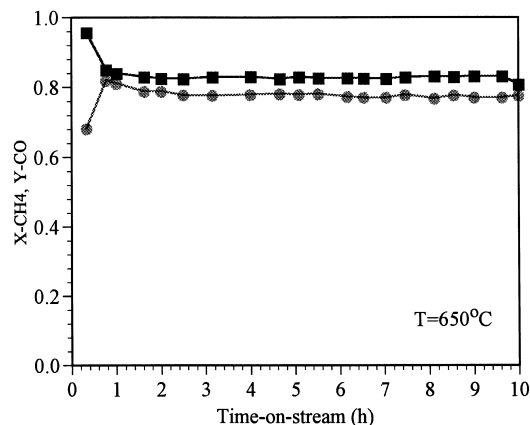


Fig. 8. Catalytic activity and stability of 5 at.% Ni-Ce(La) O_x at $T = 650^\circ\text{C}$ in a feed gas with CH $_4$ /O $_2 = 2.4$ (■) X-CH $_4$; (●) Y-CO (3.6% CH $_4$, 0.18 g s/cm 3 (STP)).

The contact time was varied in the range 0.54–0.04 g s/cm 3 (STP). Since the density of this material is ~ 2 g/cm 3 , this corresponds to a range of 270–20 ms in space time. Neither the methane conversion nor the syngas selectivity were affected by this wide change of contact time. Thus, even at ~ 20 ms space time, the equilibrium conversion is attained (Fig. 6).

The 5 at.% Ni-Ce(La) O_x catalyst showed a very stable performance at 650°C with a stoichiometric CH $_4$ /O $_2$ feed ratio of 2 at a contact time of 0.18 g s/cm 3 , as shown in Fig. 7. No deactivation was observed during 100 h-on-stream. Methane conversion and CO yield were maintained at ~ 90 and 82%, respectively. Since carbon deposition is expected to occur easily at higher methane to oxygen ratio [43], this material was also tested in a feed gas with CH $_4$ /O $_2 = 2.4$. During 10 h-on-stream, no change in methane conversion and CO yield was observed, as shown in Fig. 8. The CO selectivity was higher than 93%, while the H $_2$ /CO ratio remained equal to 2 at these conditions.

3.2. Temperature-programmed reduction by methane

As shown in Fig. 4, syngas was produced on Ce(La) O_x above 700°C , consistent with the result of Otsuka et al. [33–35]. In the presence of a small amount of nickel, as in 5 at.% Ni-Ce(La) O_x , Fig. 4, the onset of syngas formation shifted to the much lower temperature of 550°C . This may be correlated with the different reducibility of the two materials.

The reducibility of ceria-based materials by methane was thus studied by CH $_4$ -TPR, in both the TGA and the reactor-MS system. Fig. 9a shows the CH $_4$ -TPR profile of Ce(La) O_x obtained in the reactor-MS. The production of hydrogen and carbon monoxide was observed on Ce(La) O_x at $T > 650^\circ\text{C}$, coinciding with the temperature of syngas formation in POM over Ce(La) O_x , Fig. 4. At lower temperature, only CO $_2$ is formed, beginning at $\sim 600^\circ\text{C}$, which coincides with the onset of decrease of the methane signal (followed by $m/e = 15$). Therefore, at low temperature, the interaction of methane with the surface oxygen of ceria leads to complete oxidation of methane to CO $_2$ and H $_2$ O, as previously reported [24,44]. As the temperature is increased, ceria is reduced and CO and H $_2$ are formed [33–35].

The CH $_4$ -TPR profile of 5 at.% Ni-Ce(La) O_x shows that a significant amount of hydrogen and CO was produced at $\sim 525^\circ\text{C}$, coinciding with a sharp decrease of the methane signal (Fig. 9b). This can be attributed to dissociation of methane on nickel metal. In a CH $_4$ -TPR experiment with the same material carried out in the TGA, a sharp weight change at 510°C was observed. This was also observed with the 10 at.% Ni/Ce(La) O_x material. The sharp weight decrease of Ni-Ce(La) O_x observed in the TGA was attributed to reduction of NiO and the ceria support by hydrogen produced from the decomposition of methane on the freshly formed nickel metal. NiO may also be reduced by CO, which is formed by subsequent reaction of

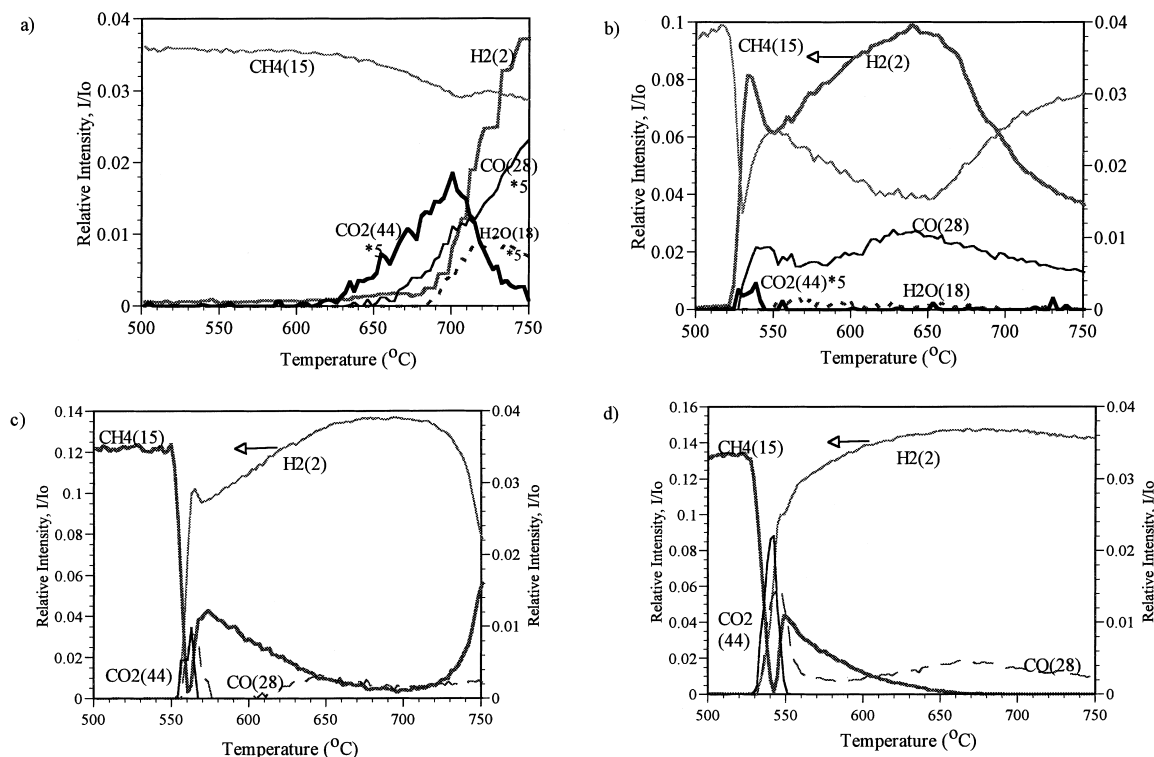


Fig. 9. CH₄-TPR of Ce(La)O_x and Ni-Ce(La)O_x followed by MS (a) Ce(La)O_x; (b) 5 at.% Ni-Ce(La)O_x; (c) 10 at.% Ni/Ce(La)O_x; (d) 20 at.% Ni/Ce(La)O_x (2% CH₄-He, 10°C/min, 50 cm³/min (STP)).

surface carbon species (from methane decomposition) with oxygen species, and form CO₂. At temperatures higher than 600°C, another peak starts to appear in CH₄-TPR, as shown in Fig. 9b, due to the participation of ceria. A measure of the reduction extent by methane is given by the value of x in CeO _{x} in CH₄-TPR carried out in the TGA, as shown in Table 3. Above 530°C,

Ni-Ce(La)O_x is more reducible than Ce(La)O_x, as shown by the reduction extent (after accounting for complete nickel oxide reduction) given in Table 3.

The CH₄-TPR profiles of 10 at.% Ni and 20 at.% Ni/Ce(La)O_x are similar to that of 5 at.% Ni-Ce(La)O_x, as shown in Fig. 9c and d. However, more methane was consumed by these two samples than by 5 at.% Ni-Ce(La)O_x, as indicated by lower CH₄ and higher H₂ values measured on these samples at temperatures above 550°C. Especially with 20 at.% Ni/Ce(La)O_x, methane was almost completely consumed at 650°C, even when the inlet methane concentration was doubled.

On the basis of the TPR results, methane activation takes place on Ni-CeO₂ catalysts at a temperature of ~550°C, which also is the light-off temperature of POM over these materials. H₂ is formed from decomposition of methane, while CO is formed by the subsequent reaction of carbon species with surface oxygen species and the bulk lattice oxygen of ceria.

Table 3
Reduction extent of cerium oxide in CH₄-TPR^a

Sample	Temperature (°C)					
	200	300	400	530	600	650
CeO ₂	2.00	1.99	1.99	1.98	1.96	1.95
5 at.% Ni-CeO ₂ ^b	2.00	2.00	2.00	1.97	1.86	1.82
Ce(La)O _x	2.00	2.00	1.99	1.98	1.97	1.96
5 at.% Ni-Ce(La)O _x ^b	2.00	2.00	2.00	1.96	1.87	1.83

^a TPR conditions: 5% CH₄-He, 10°C/min, in the TGA.

^b Reduction extent expressed as x in CeO _{x} after accounting for NiO assuming that all NiO was reduced to metallic nickel.

The enhanced POM activity of nickel-containing ceria can be attributed to the high activity of nickel in methane decomposition [45] and enhanced reducibility of ceria by methane in the presence of nickel (Table 3).

Although all Ni–Ce(La)O_x samples had similar CH₄–TPR profiles, the low-content nickel catalysts, comprising highly dispersed nickel particles in ceria, were more active/selective in POM. Similar observations have been reported by Hayakawa et al. [20] for Ni/Ca_{1-x}Sr_xTiO₃ catalysts, Chu et al. [14] for Ni/Ce/Al₂O₃, and Yan et al. [46] for Pt/CeO₂–Al₂O₃. Using in-situ XPS, Ramaroson et al. [47] have reported that Ni/CeO₂ (~2 wt.% Ni) with high metal dispersion (~57%), as determined by a magnetic measurement, caused a greater reducibility of the ceria support during reduction by H₂ than materials with lower nickel dispersion (~38%). Our H₂–TPR results [48] also suggest a higher reducibility of 5 at.% Ni–Ce(La)O_x compared to 10 at.% Ni/Ce(La)O_x, as indicated by a higher reduction extent of ceria in the presence of 5 at.% nickel at low temperatures (<300°C).

Ce³⁺ and oxygen anion vacancies were suggested by Otsuka et al. [35] to be active for H₂ and CO formation from the reaction of methane with ceria. The lattice oxygen of ceria used for the formation of CO in the absence of gaseous oxygen. Ce(Zr)O₂, which has higher oxygen ion conductivity than ceria, was reported to have a higher H₂ and CO production rate from methane beginning at lower temperatures (~600°C) than ceria [49]. Therefore, the enhanced reducibility of ceria in Ni–Ce(La)O_x with high nickel dispersion may contribute to the higher POM activity displayed by this material. On the other hand, the presence of nickel is essential for POM. A similar system, Cu–Ce(La)O_x, which is equally or more reducible than Ni–Ce(La)O_x, as suggested by previous work in our lab [44,50], is an active catalyst for the total oxidation of methane. Almost no POM activity was observed over Cu–Ce(La)O_x in the temperature range 500–700°C even under fuel-rich conditions (CH₄/O₂ = 2). This is due to the fact that copper is not active for methane dissociation [45]. The lattice oxygen of CuO is an active site for the complete oxidation of CH₄ [51]. On the other hand, nickel catalyzes the dissociation of methane [52,53]

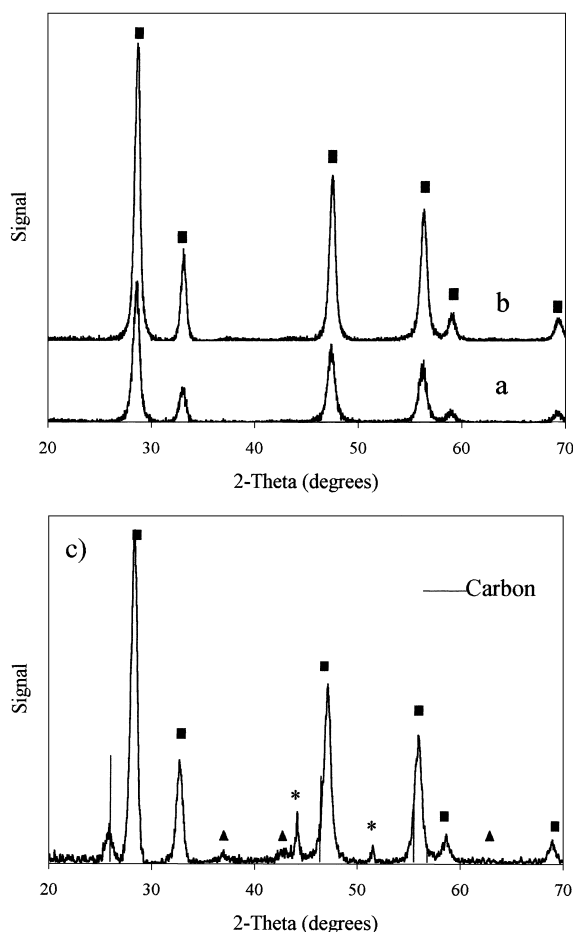


Fig. 10. XRD patterns of used (a) 5 at.% Ni–Ce(La)O_x (after 100 h-on-stream at 650°C); (b) 10 at.% Ni/Ce(La)O_x and (c) 20 at.% Ni/Ce(La)O_x (after 550–700°C for a total of 16 h, 3% CH₄–1.5% O₂–He, 0.18 g s/cm³ (STP)); (■) CeO₂; (▲) NiO; (★) Ni.

3.3. Characterization of used samples

After 100 h-use at 650°C (Fig. 7), no change in the XRD patterns was observed for the 5 at.% Ni–Ce(La)O_x sample, as shown in Fig. 10. However, the particle size of CeO₂ obtained from CeO₂ (1 1 1) reflections is bigger than that of the fresh sample (Table 1), suggesting that crystal growth took place during the 100 h-on-stream. The surface area of this used material is ~27 m²/g, much lower than that of the fresh sample but slightly higher than that of used Ce(La)O_x (Table 1). The growth of ceria particle size

was much faster for the high Ni-content ceria, and resulted in low surface area after only 16 h-on-stream up to 700°C, as shown in Table 1. Fig. 10c shows that both NiO and metallic Ni phases were present in 20 at.% Ni/Ce(La)O_x after only 16 h-use up to 700°C (under the conditions of Fig. 5). Therefore, NiO in the catalyst was partially reduced to metallic nickel during reaction. The catalyst is active and selective in this partially reduced form. This can also explain the observed hysteresis behavior of this catalyst in POM. Furthermore, new reflections appeared in the XRD pattern of the used catalyst in Fig. 10c. These are assigned to graphitic carbon. Thus, carbon deposition took place during POM on this catalyst. This explains the poor carbon balance obtained in the test shown in Fig. 5 for 20 at.% Ni/Ce(La)O_x.

STEM/EDS elemental mapping of the 5 at.% Ni–Ce(La)O_x sample after 100 h-on-stream indicates that some agglomeration of nickel particles took place during reaction, as shown in Fig. 11a. However, dispersed nickel is still prevailing in this material. On the other hand, agglomeration of nickel particles was very severe in the 10 at.% Ni/Ce(La)O_x sample after 16 h-use up to 700°C, as shown in Fig. 11b.

The surface composition of 5 at.% Ni–Ce(La)O_x after 100 h-on-stream at 650°C was analyzed by XPS. Fig. 12 shows the O1s and C1s spectra of this sample and of the as-prepared 5 at.% Ni–CeO₂ for comparison. The O1s spectra show two peaks at 529.1 and 532.2 eV on both the used and as-prepared materials (Fig. 12). These are assigned to metal oxides and surface carbonate [54], respectively. C1s spectra show a prominent peak at a binding energy of 284.6 eV which is assigned to residual hydrocarbons. A small peak at

288.5 eV, which was also observed on the fresh materials, may be due to residual surface CO₃²⁻. There was no peak due to graphitic or carbidic surface carbon species, whose binding energy is at ~283 eV [54]. The deconvolution of the C1s signal of used 5 at.% Ni–Ce(La)O_x, gave a dominant peak of FWHH (full width at half height) = 1.8 eV at 284.6 eV and a component at 283.03 eV with 8% of the total carbon signal, close to that on the fresh material. Therefore, XPS found no carbon on the surface of 5 at.% Ni–Ce(La)O_x even after 100 h-on-stream at 650°C.

3.4. Temperature programmed oxidation

Potential carbon deposition during POM was further checked by TPO of used samples. Fig. 13 shows the TPO curves of used Ni–Ce(La)O_x catalysts obtained in the TGA. Two peaks centered at the temperatures of 320 and 500°C were observed for 10 at.% Ni/Ce(La)O_x, while only one peak at 550°C was found in the TPO curve of 20 at.% Ni/Ce(La)O_x. TPO was also conducted in the microreactor with the product gas monitored for CO₂ by the NDIR analyzer. The analysis confirmed that these peaks were due to production of CO₂. The weight loss in TPO of used samples in the TGA is shown in Table 4. These values represent a lower bound to carbon deposition on the catalysts, as discussed below. The total carbon deposition, 0.18 g (carbon)/g (catalyst), on the 20 at.% Ni/Ce(La)O_x catalyst is comparable to that on the 13 wt.% Ni/CeO₂ (6 h at 750°C), 0.13 g (carbon)/g (catalyst), reported by Tang et al. [17], and it is much higher than that on the 10 at.% Ni/Ce(La)O_x catalyst, 0.029 g (carbon)/g (catalyst).

Table 4
TPO^a-weight change of catalysts used in POM^b

Sample	Reaction conditions	Weight loss (wt.%) ^c
5 at.% Ni–Ce(La)O _x	0.12 g s/cm ³ , up to 700°C, 16 h	0.064
	0.18 g s/cm ³ , at 650°C, 100 h	0.10
	0.04 g s/cm ³ , up to 700°C, 16 h	0.064
	CH ₄ /O ₂ = 2.4, 0.18 g s/cm ³ , at 650°C, 10 h	0.42
10 at.% Ni/Ce(La)O _x	0.36 g s/cm ³ , up to 700°C, 16 h	2.90
20 at.% Ni/Ce(La)O _x	0.18 g s/cm ³ , up to 700°C, 16 h	18.00

^a TPO was performed in the TGA in 5% O₂–He at a flow rate of 200 cm³/min, heating rate 5°C/min over the temperature range 25–800°C.

^b Unless otherwise specified, all POM tests were run with a feed gas ratio of CH₄/O₂ = 2.

^c This represents a lower bound to the carbon deposited on each sample (see text), 10² g (carbon)/g (catalyst).

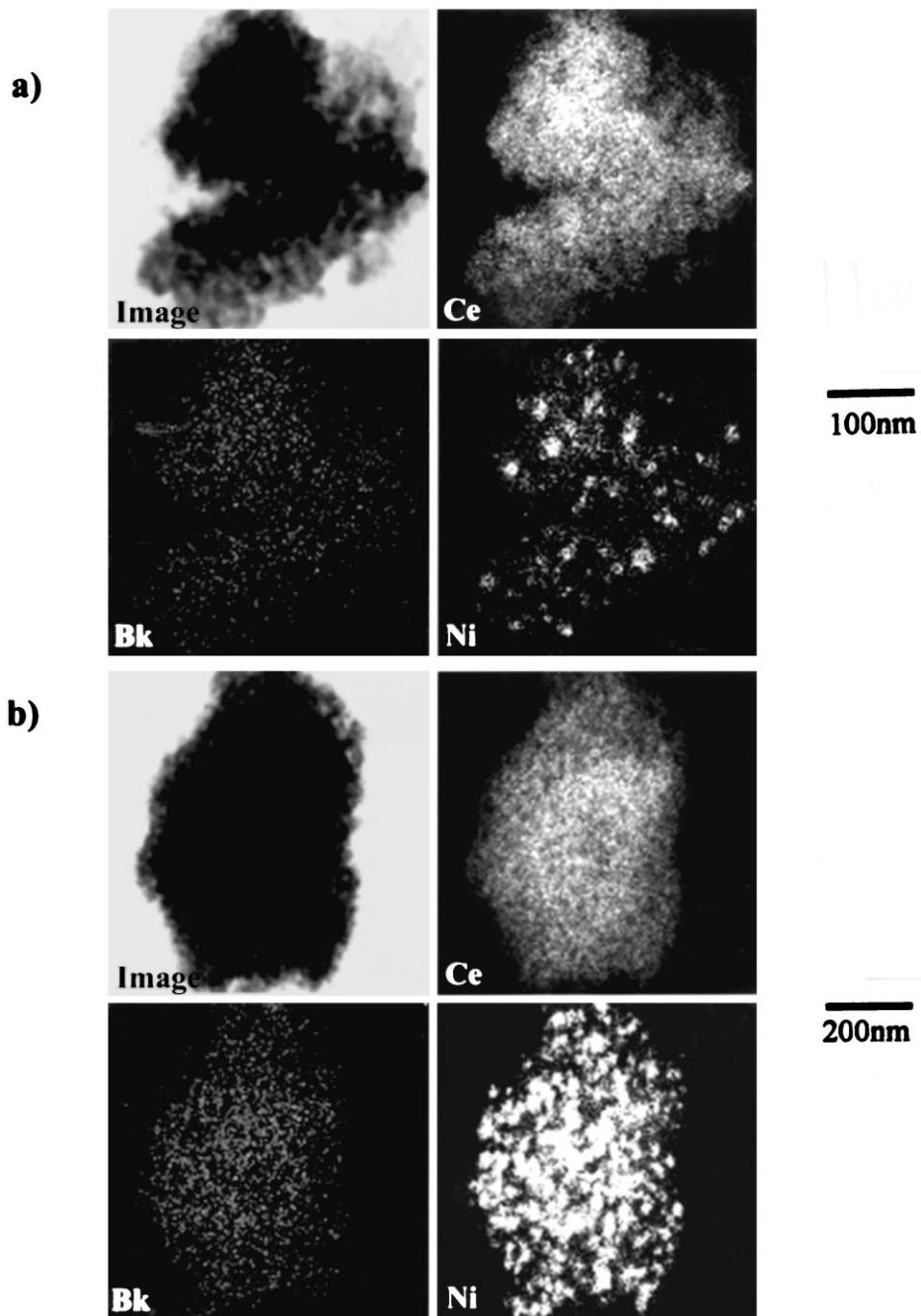


Fig. 11. STEM/EDS of used (a) 5 at.% Ni-Ce(La) O_x ; (b) 10 at.% Ni/Ce(La) O_x .

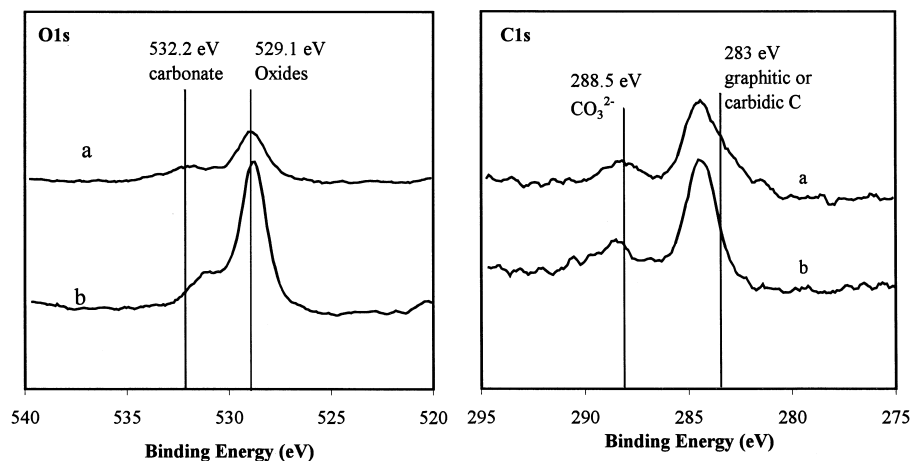


Fig. 12. O1s and C1s XP spectra of (a) used 5 at.% Ni-Ce(La)O_x (100 h-on-stream at 650°C); (b) as-prepared 5 at.% Ni-CeO₂.

On the other hand, for the used 5 at.% Ni-Ce(La)O_x at all conditions, including after 100 h-on-stream, no peak was found in the TGA-TPO experiments over the temperature range of 25–800°C, and also no CO₂ was eluted in the TPO run in the reactor-IR system. The TGA-TPO data are shown in Table 4. Even after testing this material at 650°C for 10 h with a higher CH₄/O₂ feed ratio (CH₄/O₂ = 2.4), which would accelerate the carbon deposition process, no significant

weight change (0.0042 g (carbon)/g (catalyst)) was observed. Therefore, the 5 at.% Ni-Ce(La)O_x material, which contains highly dispersed nickel, is resistant to carbon deposition.

Ceria may be in a partially reduced state during the POM tests. The reoxidation of ceria will cause a weight increase in the TGA-TPO experiments, while the oxidation of deposited carbon species causes a weight decrease. The real weight change due to the

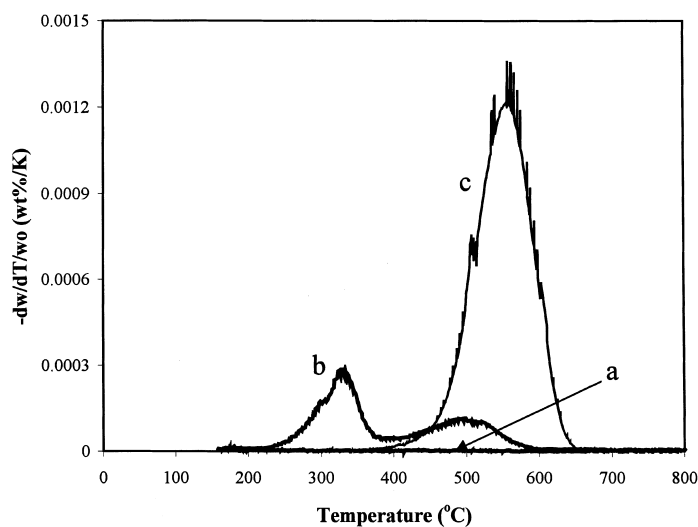


Fig. 13. TPO of used Ni-Ce(La)O_x catalysts in the TGA, (a) 5 at.% Ni-Ce(La)O_x; (b) 10 at.% Ni-Ce(La)O_x; (c) 20 at.% Ni-Ce(La)O_x (5°C/min, 10% O₂-He, 200 cm³/min).

oxidation of carbon is, thus, the sum of the observed weight loss and the weight change due to reoxidation of ceria. Therefore, the data shown in Table 4, based on the recorded sample weight loss in the TGA, represents a lower bound for the carbon deposition on these catalysts. However, for the 5 at.% Ni–Ce(La)O_x sample, we can say with certainty that no carbon was deposited, because also no CO₂ was eluted during the TPO run in the reactor-IR system. XPS analysis of the 100 h-used sample verified that it was free of carbon.

In general, a high degree of metal dispersion may reduce coke formation [43]. Perovskite-supported nickel catalysts with high dispersion of nickel have been reported to be more stable in POM due to their enhanced resistance to carbon deposition [18,20]. Recently, it has been shown that the resistance of Ni/Al₂O₃ catalysts to carbon deposition can be improved by addition of a rare earth metal oxide (La, Ce, Y) [11,12,14]. The additive was proposed to improve the dispersion of nickel. From the present work, a similar conclusion may be reached for the Ni–CeO₂ system. STEM/EDS has shown that nickel in the 5 at.% Ni–Ce(La)O_x catalyst is highly dispersed in the ceria matrix, while XPS analysis indicates no surface enrichment of nickel in Ni–Ce(La)O_x with nickel loadings up to 10 at.%. With high Ni-loading, both dispersed nickel and bulk NiO particles were found in the catalyst and the surface was enriched in nickel. The performance of these catalysts was more like that of bulk nickel oxide, thus, resulting in carbon deposition.

On the other hand, the oxygen mobility of ceria may also contribute to the high carbon resistance of 5 at.% Ni–Ce(La)O_x. Ceria is well known for its high oxygen storage capacity and oxygen mobility, which can be further enhanced in the presence of dopants or metals. The work carried out in our lab has shown higher reducibility of La-doped ceria compared to undoped ceria, and even higher reducibility caused by the addition of Cu or Ni in Ce(La)O_x [24,25,48]. Our CH₄-TPR results also show that Ni-containing ceria is more reducible by methane than ceria (Table 3). The high oxygen mobility of ceria may accelerate the surface oxidation reactions of carbon by reactive oxygen species, thus, inhibiting carbon growth on the catalyst surface. A similar reasoning may be applied to perovskite-supported nickel as perovskite-type oxides are well-known oxygen ion conductors [55]. For modified Ni/Al₂O₃, the addition of cerium or other

rare earth oxides may increase the available surface oxygen of alumina, thus, providing a higher rate of carbon oxidation.

4. Conclusions

Ni-containing ceria, with nickel content in the range of 5–20 at.% (2.5–10 wt.%), is a highly active and selective catalyst for partial oxidation of methane to syngas at temperatures higher than 550°C. However, only the 5 at.% Ni–Ce(La)O_x material with high nickel dispersion in ceria showed excellent resistance to carbon deposition and, thus, had a high stability under reaction conditions. In contrast, carbon deposition occurred on high nickel-containing ceria, which comprised both dispersed nickel and bulk nickel oxide particles. Pre-reduction was not necessary to activate the highly dispersed 5 at.% Ni–Ce(La)O_x, while 20 at.% Ni/Ce(La)O_x, if used in the unreduced state, showed a higher light-off temperature and hysteresis. The reduction onset temperature of Ni–Ce(La)O_x in CH₄-TPR is lower than that of CeO₂ or Ce(La)O_x and correlates well with the onset of POM on this catalyst. The synergistic effect of the highly dispersed nickel-ceria system is attributed to the facile transfer of oxygen from ceria to the nickel interface, effectively oxidizing any carbon species produced from methane dissociation on nickel.

Acknowledgements

We wish to acknowledge the assistance of Dr. Anthony Garratt-Reed and Ms. Elisabeth Shaw of the Center for Materials Science and Engineering at the Massachusetts Institute of Technology, with the STEM/EDX and XPS analysis, respectively. We also thank the reviewers of the paper.

References

- [1] A.T. Ashcroft, A.K. Cheetham, J.S. Ford, M.L.H. Green, C.P. Grey, A.J. Murrel, P.D.F. Vernon, *Nature* 344 (1990) 319.
- [2] M. Prettre, C.H. Eichner, M. Perrin, *Trans. Faraday Soc.* 43 (1946) 335.
- [3] W.J.M. Vermeiren, E. Blomsma, P.A. Jacobs, *Catal. Today* 13 (1992) 427.
- [4] T. Hayakawa, A.G. Andersen, M. Shimizu, K. Suzuki, K. Takehira, *Catal. Lett.* 22 (1993) 307.

- [5] D. Dissanayake, M.P. Rosynek, K.C.C. Kharas, J.H. Lunsford, *J. Catal.* 132 (1991) 117.
- [6] P.D.F. Vernon, M.L.H. Green, A.K. Cheetham, A.T. Aschcroft, *Catal. Lett.* 6 (1990) 181.
- [7] R.H. Jones, A.T. Aschcroft, D. Waller, A.K. Cheetham, J.M. Thomas, *Catal. Lett.* 8 (1991) 169.
- [8] D.A. Hickman, L.D. Schmidt, *Science* 259 (1993) 343.
- [9] P.M. Torniainen, X. Chu, L.D. Schmidt, *J. Catal.* 146 (1994) 1.
- [10] J.B. Claridge, M.L.H. Green, S.C. Tsang, A.P.E. York, A.T. Aschcroft, P.D. Battle, *Catal. Lett.* 22 (1993) 299.
- [11] Q. Miao, G. Xing, S. Sheng, W. Cui, L. Xu, X. Guo, *Appl. Catal. A* 154 (1997) 17.
- [12] L. Cao, Y. Chen, W. Li, *Stud. Surface Sci. Catal.* 107 (1997) 467.
- [13] Q.G. Yan, W. Chu, L.Z. Gao, Z.L. Yu, S.Y. Yuan, *Stud. Surface Sci. Catal.* 119 (1998) 855.
- [14] W. Chu, Q. Yan, X. Liu, Z. Yu, G. Xiong, *Stud. Surface Sci. Catal.* 119 (1998) 849.
- [15] V.R. Choudhary, B.S. Uphade, A.S. Mamman, *J. Catal.* 172 (1997) 281.
- [16] E. Ruckenstein, Y.H. Hu, *Appl. Catal. A* 183 (1999) 85.
- [17] S. Tang, J. Lin, K.L. Tan, *Catal. Lett.* 51 (1998) 169.
- [18] R. Shiozaki, A.G. Andersen, T. Hayakawa, S. Hamakawa, K. Suzuki, M. Shumizu, K. Takehira, *J. Chem. Soc., Faraday Trans.* 93 (1997) 3235.
- [19] P. Chen, H.B. Zhang, G.D. Lin, K.R. Tsai, *Appl. Catal. A* 166 (1998) 343.
- [20] T. Hayakawa, H. Harihara, A.G. Andersen, K. Suzuki, H. Yasuda, T. Tsunoda, S. Hamakawa, A.P.E. York, Y.S. Yoon, M. Shimizu, K. Takehira, *Appl. Catal. A* 149 (1997) 391.
- [21] H.C. Yao, Y.F.Y. Yao, *J. Catal.* 86 (1984) 254.
- [22] B. Harrison, A.F. Diwell, C. Hallett, *Platinum Met. Rev.* 32 (1988) 73.
- [23] A. Trovarelli, G. Dolcetti, C.de. Leitenburg, J. Kašpar, *Stud. Surface Sci. Catal.* 75 (1993) 2781.
- [24] Lj. Kundakovic, M. Flytzani-Stephanopoulos, *Appl. Catal. A* 171 (1998) 13.
- [25] W. Liu, M. Flytzani-Stephanopoulos, *Chem. Eng. J.* 64 (1996) 283.
- [26] G. Wrobel, C. Lamonier, A. Bennani, A. D'Huysser, A. Aboukais, *J. Chem. Soc., Faraday Trans.* 92 (1996) 2002.
- [27] C. Lamonier, A. Ponchel, A. D'Huysser, L. Jalowiecki-Duhamel, *Catal. Today* 50 (1999) 247.
- [28] O. Rienäcker, *Z. Anorg. Allg. Chem.* 258 (1949) 280.
- [29] W. Liu, M. Flytzani-Stephanopoulos, *J. Catal.* 153 (1995) 304.
- [30] W. Liu, M. Flytzani-Stephanopoulos, *J. Catal.* 153 (1995) 317.
- [31] C. Hardacre, R.M. Ormerod, R.M. Lambert, *J. Phys. Chem.* 98 (1994) 10901.
- [32] E. Zamar, A. Trovarelli, C. de Leitenburg, G. Dolcetti, *J. Chem. Soc., Chem. Commun.* (1995) 965.
- [33] K. Otsuka, T. Ushiyama, I. Yamanaka, *Chem. Lett.* (1993) 1517.
- [34] K. Otsuka, E. Sunada, T. Ushiyama, I. Yamanaka, *Stud. Surface Sci. Catal.* 107 (1997) 531.
- [35] K. Otsuka, Y. Wang, E. Sunada, I. Yamanaka, *J. Catal.* 175 (1998) 152.
- [36] S. Wang, G.Q. Lu, *Appl. Catal. B* 19 (1998) 267.
- [37] S.M. Stagg, D.E. Resasco, *Stud. Surface Sci. Catal.* 119 (1998) 813.
- [38] Y. Amenomiya, A. Emesh, K. Oliver, G. Pleizer, in: M. Philips, M. Ternan (Eds.), *Proceedings of the Ninth International Congress Catalyst Chemical Institute of Canada, Ottawa, Canada, 1988*, p. 634.
- [39] T. Zhu, A. Dreher, M. Flytzani-Stephanopoulos, *Appl. Catal. B* 21 (1999) 103.
- [40] Available through the web: stokes.lance.colostate.edu.
- [41] S.C. Tsang, J.B. Claridge, M.L.H. Green, *Catal. Today* 23 (1995) 3.
- [42] V.R. Choudhary, A.M. Rajput, V.H. Rare, *J. Phys. Chem.* 96 (1992) 8686.
- [43] C.H. Bartholomew, *Catal. Rev.-Sci. Eng.* 24 (1982) 67.
- [44] Lj. Kundakovic, M. Flytzani-Stephanopoulos, *J. Catal.* 179 (1998) 203.
- [45] M.S. Liao, C.T. Au, C.T. Ng, *Chem. Phys. Lett.* 272 (1997) 445.
- [46] Q.G. Yan, W. Chu, L.Z. Gao, Z.L. Yu, S.Y. Yuan, *Stud. Surface Sci. Catal.* 119 (1998) 855.
- [47] E. Ramarosan, J.F. Tempere, M.F. Guilleux, F. Vergand, H. Roulet, G. Dufour, *J. Chem. Soc., Faraday Trans.* 88 (1992) 1211.
- [48] T. Zhu, Ph.D. Thesis, Department of Chemical Engineering, Tufts University, Medford, MA, 2000.
- [49] K. Otsuka, Y. Wang, M. Nakamura, *Appl. Catal. A* 183 (1999) 317.
- [50] Y. Li, M.S. Thesis, Department of Chemical Engineering, Tufts University, Medford, MA, 1998.
- [51] C.T. Au, H.Y. Wang, H.L. Wan, *J. Catal.* 158 (1996) 343.
- [52] C.T. Au, Y.H. Hu, H.L. Wan, *Catal. Lett.* 27 (1994) 199.
- [53] C.T. Au, Y.H. Hu, H.L. Wan, *Catal. Lett.* 36 (1996) 159.
- [54] *Handbook of X-ray Photoelectron Spectroscopy*, Perkin-Elmer, Physical Electronics Division, 1978.
- [55] N.Q. Minh, *J. Am. Ceram. Soc.* 76 (3) (1993) 563.
- [56] R. Jenkins, R.L. Snyder, *Introduction to X-ray Diffractometry*, Wiley, New York, 1996.